



This is the accepted manuscript made available via CHORUS. The article has been published as:

Thermal Convection in a Central Force Field Mediated by Sound

John P. Koulakis, Yotam Ofek, Seth Pree, and Seth Putterman

Phys. Rev. Lett. **130**, 034002 — Published 20 January 2023

DOI: [10.1103/PhysRevLett.130.034002](https://doi.org/10.1103/PhysRevLett.130.034002)

Thermal convection in central force field mediated by sound

John P. Koulakis^{1,*}, Yotam Ofek¹, Seth Pree^{1,2}, and Seth Putterman¹

¹ *Department of Physics and Astronomy, University of California Los Angeles, Los Angeles, California 90095, USA and*

² *Present Address: Applied Physics and Materials Science, California Institute of Technology, Pasadena, California 91125, USA.*

(Dated: November 18, 2022)

Convection in radial force fields is a fundamental process behind weather on the Earth and Sun, as well as magnetic dynamo action in both. Until now, benchtop experiments have been unable to study convection in radial force fields due to the inability to generate radial forces of sufficient strength. Recently, it has been appreciated that sound, when averaged over many cycles, exerts a force on density gradients in the gas it travels through. The acoustic radiation pressure on thermal gradients draws cooler gas to regions with large time-averaged acoustic velocity and can be modeled as an effective acoustic gravity. We have constructed a system which generates a high amplitude, spherically symmetric acoustic wave in a rotating spherical bulb containing weakly ionized sulfur gas. Without sound, the gas stratifies itself into an initial state with the warmest gas near the center of the bulb, and the coolest gas near the bulb surface. When the sound is initiated, the acoustic radiation pressure is not balanced and a convective instability is triggered. With high speed videography, we observe the initial shape and growth rate of the most unstable mode at various acoustic amplitudes. Acoustic and rotational forces both contribute to the detailed mode shape, which changes qualitatively at low amplitudes where acoustic forces no longer surpass rotational ones everywhere in the bulb.

INTRODUCTION

Convection in spherical, rotating, systems is fundamental to processes in stars and planets and is ubiquitous throughout our universe. It partially determines, for example, solar flares and space weather [1], granulation on the sun’s surface [2], weather on the Earth, and magnetic dynamo action in both [3, 4]. Convection experiments in spherical systems with a radial force are difficult to realize due to the challenges of arranging for a radial force that overwhelms buoyancy (gravity) at the Earth’s surface. To date, the only viable option has been the dielectrophoretic force, which relies on strong alternating electric fields and variations in a fluid’s dielectric constant with temperature [5–8]. However, because of its inherent weakness, experiments were forced into a microgravity environment, with all associated challenges and expenses [9–13].

Recent advances in generalizing acoustic radiation pressure theory to encompass inhomogeneous fluids [14, 15] have found that sound exerts a non-zero, time-averaged force on density *gradients*. In the simplest case of an ideal gas, the leading order slow dynamics are described by [14, 16],

$$\frac{\partial}{\partial t} (\bar{\rho} \bar{\mathbf{v}}) + \nabla (\bar{\rho} \bar{\mathbf{v}} \bar{\mathbf{v}}) = -\nabla \bar{P}^{\text{eff}} - \frac{\langle v_1^2 \rangle}{2} \nabla \bar{\rho} + \bar{\rho} \mathbf{g} + \eta \nabla^2 \bar{\mathbf{v}} \quad (1)$$

where $\bar{\rho}$, \bar{P}^{eff} , $\bar{\mathbf{v}}$ are the time-averaged density, effective pressure, and velocity respectively, \mathbf{g} is a gravitational field, $\langle v_1^2 \rangle$ is the time-averaged square of the acoustic velocity, and η is the viscosity. Aside from a modification of the pressure, the sound field, at second order, leads to a pycnoclinic acoustic radiation force given by $-\langle v_1^2 \rangle \nabla \bar{\rho} / 2$. That this term leads to an acoustic gravity

$\mathbf{g}_{ac} = \nabla \langle v_1^2 \rangle / 2$ can be motivated by taking the curl of equation 1 neglecting viscosity and convection to obtain,

$$\frac{\partial}{\partial t} \nabla \times (\bar{\rho} \bar{\mathbf{v}}) = [\mathbf{g} + \nabla \langle v_1^2 \rangle / 2] \times \nabla \bar{\rho}, \quad (2)$$

and noting that $\nabla \langle v_1^2 \rangle / 2$ generates vorticity in the same manner as \mathbf{g} . This argument is equivalent to that made for thermovibrational [17] and dielectrophoretic [8–10] forces, where, in particular, the force on dielectric gradients $-E^2 \nabla \epsilon / 2$ for permittivity ϵ and electric field E forms the basis of the “electrostatic gravity” $\epsilon \nabla E^2 / 2$ in the microgravity experiments. In the case of acoustic gravity, dense gas falls towards regions of high acoustic velocity, and with a spherical standing wave, one can arrange for an acoustic gravity that points radially.

Herein we describe experiments on convective instability triggered by the turn-on of a radial acoustic gravity field. Figure 1a is one frame of a high speed video capturing the flow of hot sulfur gas immediately after a spherical acoustic wave is excited in a 3 cm diameter bulb that simultaneously rotates. The overlaid convection cells are axisymmetric and determined by studying videos available in the supplementary material.

The sulfur gas is heated volumetrically by microwaves. Sound is excited by amplitude modulating the microwave, and can briefly reach amplitudes that imply an acoustic gravity field that is $\sim 1000\times$ stronger than Earth’s gravity [18]. As shown in figure 1b, the lowest order spherically-symmetric acoustic mode has a velocity profile similar to a half-sine wave with maximum (antinode) at about half the bulb radius [19]. This means the acoustic gravity of that mode has a profile similar to a full sine wave, changing sign at the antinode. From the antinode inwards (the inner zone), the gas is stably stratified

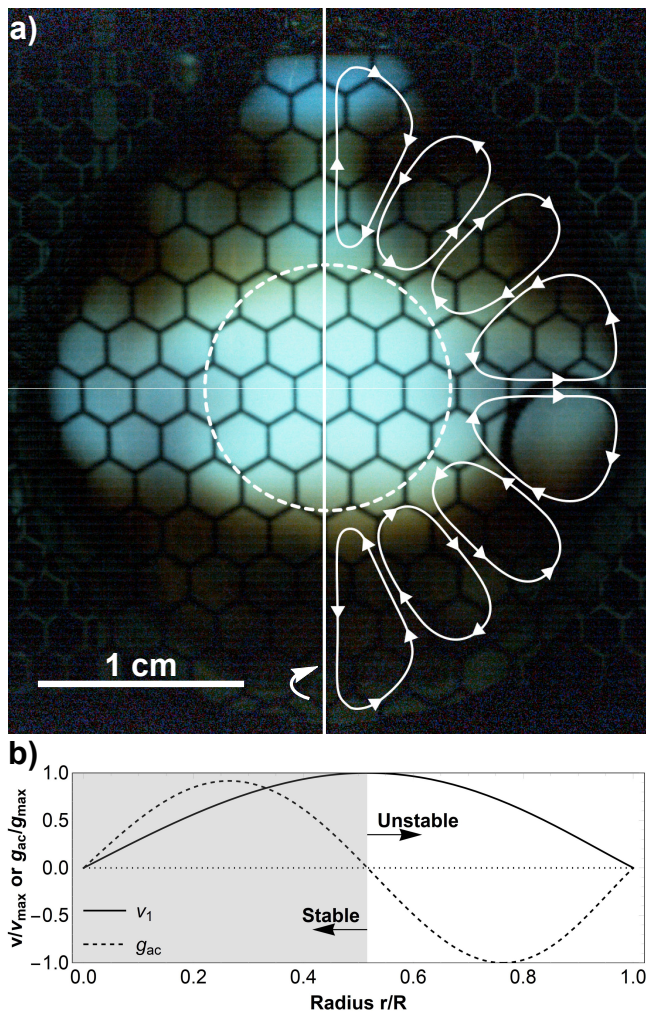


FIG. 1. a) Convection cells driven by the radial “acoustic gravity” of a spherical standing sound wave in a rotating sulfur plasma bulb. Direction of flow indicated by the streamlines has been extracted from high speed video available in the supplementary materials. Cells are axisymmetric about the rotation axis (vertical line centered in figure). The hexagonal pattern visible in the image is the shadow of the metal mesh which forms the microwave cavity. b) The acoustic velocity and effective gravity as a function of radius. Note that the acoustic gravity changes sign at the velocity antinode, which occurs at nearly half the bulb radius (dashed white circle). Since the plasma is volumetrically heated internally and is hottest at the center, the region inside of the antinode is stable, while the region outside of the velocity antinode is unstable. Convection in the outer zone is similar to Rayleigh-Bénard convection in a time-varying, spherical, acoustic gravity field.

with the hottest gas at the center. Conversely, the region from the antinode outwards (the outer zone) is characterized by instability [18] best described as Rayleigh-Bénard convection in a time-varying acoustic gravity field, but with an internal source of heat and lacking one boundary [20, 21]. Convection in the outer zone dramatically

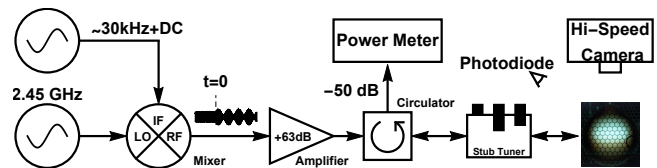


FIG. 2. Block diagram of microwave system which heats the sulfur and generates sound. Amplitude modulation of the microwave power generates sound waves inside the bulb. The acoustic gravity of the standing sound wave destabilizes the stratification of the quiescent bulb and the growth of the most unstable mode is captured on high-speed video as a function of microwave modulation depth.

increases thermal transport to the glass, resulting in a frequency shift of the resonant mode [22], and measurably hotter glass temperature [18].

This work focuses on the initial motion of the fluid immediately after exciting the sound wave to better understand the most unstable, fastest growing convective mode. We have observed the instability at various acoustic amplitudes at fixed rotation rate, and have identified a transition in the modal structure at low amplitudes. We interpret the transition in terms of a balance of acoustic and rotational forces at the equator.

EXPERIMENT

A block diagram of the experimental system is shown in figure 2. It has been described extensively in various forms elsewhere [18, 23–25] and here we describe aspects specific to this work. The plasma bulb sits inside a cylindrical microwave cavity made of hexagonal metal mesh which simultaneously confines the microwave and allows visualization of the convection. Initially, the sulfur plasma is heated by an unmodulated 2.45 GHz microwave signal amplified up to 2 kW by a solid state linear amplifier (Empower 2180) to a final molecular density of $\sim 2 \times 10^{19} \text{ cm}^{-3}$ and $\sim 10^{-5}$ ionization fraction [26, 27]. Impedance matching is achieved with a 3-stub tuner. Once quiescent conditions are reached, the acoustic resonance frequency of the bulb’s lowest order spherically symmetric mode (near 30 kHz) is determined by imposing a small $\sim 2\%$ modulation depth and sweeping the modulation frequency until the plasma is observed to flicker [19]. The spherical symmetry of the acoustic mode has been confirmed with direct observation [18] and matching of the ultrasonic resonance spectrum with theory [19]. The amplitude modulation is switched off and the plasma is allowed to return to the quiescent state. While off, the modulation frequency is set to match the resonance and the modulation depth is increased to 40-100%. A high speed video camera (Vision Research Phantom v2640) operating at 5000 frames per second begins recording and the instability is triggered by reacti-

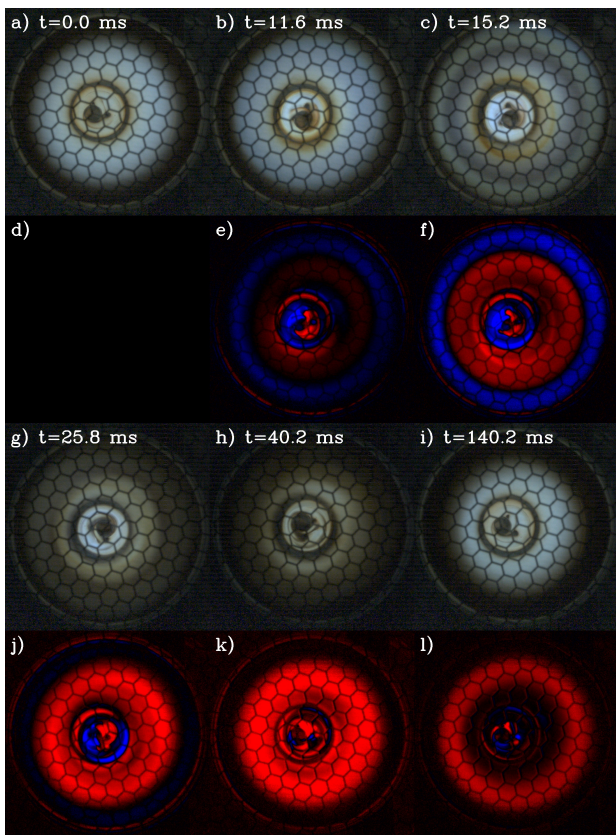


FIG. 3. Top view of instability evolution indicates the instability is axially symmetric. The feature visible at the center of the bulb in every frame is a pontil mark on the bulb from glassblowing. Panels a-c and g-i are frames of high speed video while panels d-f and j-l are false color images of the difference in brightness from panel a. Red (blue) coloring indicates the pixel value is lower (higher) than it was in panel a.

uating the modulation. The growth of the most unstable mode is captured for various acoustic amplitudes at a fixed bulb rotation rate of 17 Hz. Rotation of the bulb is essential for achieving steady-state, quiescent conditions; without it the plasma is chaotic, violently flickers, and is prone to sudden extinction [28].

RESULTS AND DISCUSSION

Figures 3 and 4 show high speed video frames from two distinct but analogous events viewed from the top (along the rotation axis) and side respectively. The first and third rows of each figure show the frames in actual color while the second and fourth rows are false color images of the difference in pixel brightness from the first frame. Panel a) in both figures shows the plasma in the quiescent state before the acoustic gravity is initiated. From the top view (figure 3) the flow is seen to be axially symmetric about the rotation axis. In panel 3b) the luminous radius of the plasma has moved out leaving

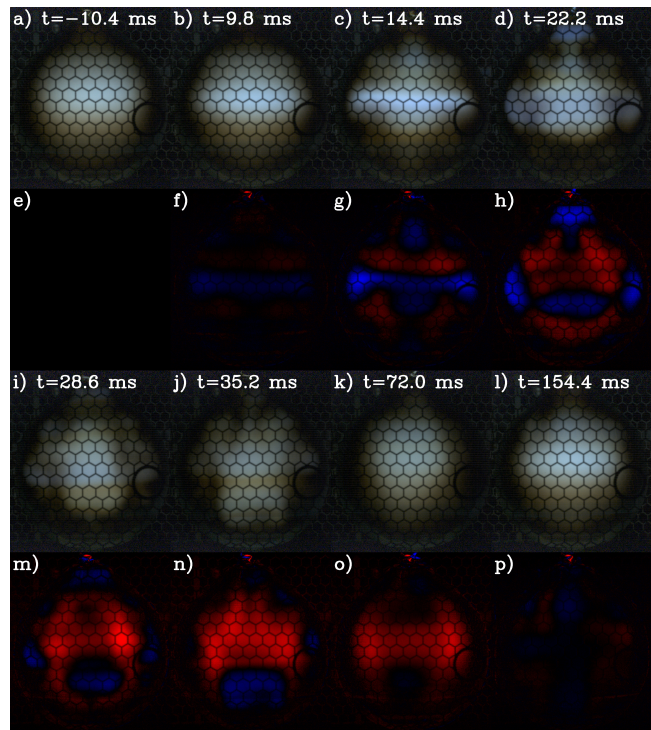


FIG. 4. Side view of instability evolution. Panels a-d and i-l are frames of high speed video while panels e-h and m-p are false color images of the difference in brightness from panel a. Red (blue) coloring indicates the pixel value is lower (higher) than it was in panel a.

dimmer pixels near the center. A clear, dim ring encircling the inner zone in 3c) indicates the outer zone has inverted bringing the hot gas towards the glass and the cooler gas towards the velocity antinode. Heat flows into the glass leaving dimmer plasma in the outer zone (3g and 3h), shifting the resonant frequency of the bulb, and detuning it from the drive. By panel 3i), the acoustic amplitude and acoustic gravity have decayed sufficiently to allow the gas to heat back up to the quiescent state. Viewing the event from the side, figure 4, elucidates the polar angular structure of the flow. The outward motion visible in 3b) and c) is outward flow at the equator. Also, there is outward flow at the poles and mid-latitudes (at about 45°) with the return flow between. The outward plumes form an 8-pointed star seen in panel 4c), some of which evolve into mushroom shaped features after interacting with the glass in panel 4d). Panels 4i)-l) show the cooling and recovery. The inner zone is distinctly visible as a bright, unmoving ball once the outer zone cools, as in figures 3h and 4d).

The axisymmetric convection cells we observe are similar in character to those predicted for thermal convec-

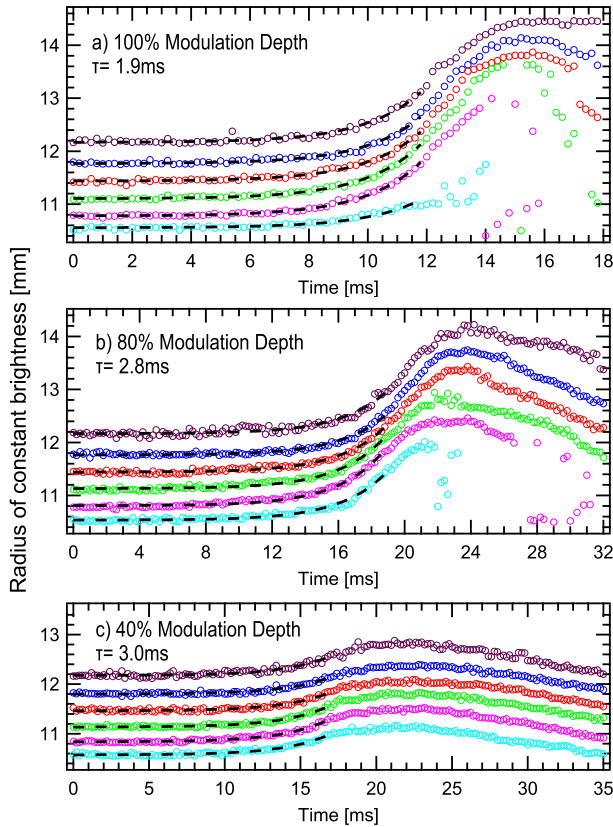


FIG. 5. Timescales of convection onset are extracted from the top view high frame rate videos by finding the radius of circles where the brightness drops below a threshold value over time and fitting exponentials (dashed black curves). Each color is a different threshold, with inner contours corresponding to higher thresholds (brighter pixels).

tion in spherical shells with normal gravity [29], and in planar systems with acoustic gravity [16]. The linear theory for the modes with spherical acoustic gravity has not been developed. Consistent formation of outward plumes at the poles and equator implies spherical symmetry has been sufficiently broken to pin the orientation of the mode. Rotation of the bulb can give a preferred direction, as can asymmetry in the quiescent state due to Earth’s gravity, asphericity of the bulb itself, wobble of the rotation axis, or small amplitudes of other acoustic modes.

Extraction of the mode’s growth time is facilitated by the symmetry of the flow when viewed from the top. An algorithm processes the videos by finding the brightness of pixels as a function of the distance from the plasma center, which is a monotonically decreasing curve at early times. It then finds the radius at which the plasma brightness drops below a set threshold. Plotting these radii over time for various thresholds or, equivalently, initial position, gives the curves in figure 5. Since the growth time of a convection mode does not vary in space,

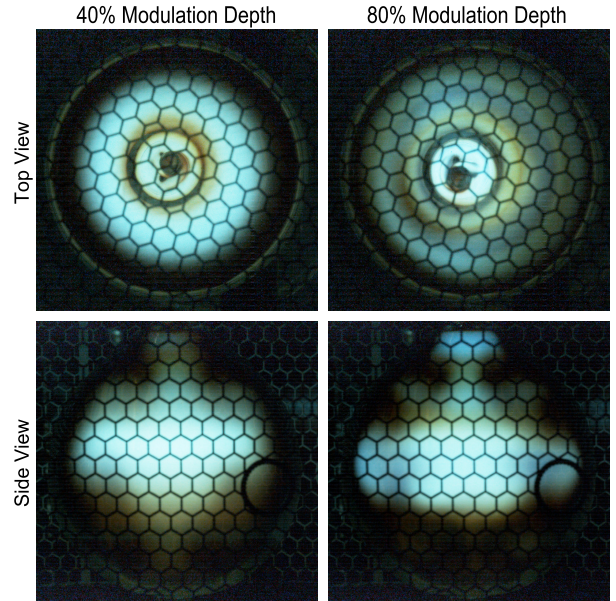


FIG. 6. Although the growth times of the convective modes at 40% and 80% modulation depth are similar, their shape is qualitatively different. This difference is due to a change in the balance of rotational and acoustic forces.

each curve must have the same time constant. To ensure this, a least squares fit is done simultaneously to all curves, forcing their time constants to be equal. The resulting fits are the dashed black curves overlaid on the data. The growth time constants are 1.9 ms, 2.8 ms, and 3.0 ms for 100%, 80%, and 40% modulation depth respectively.

Acoustic gravity and the convective growth rate (inverse time constant) are expected to scale with the square of the acoustic amplitude, or square of the modulation depth [16]. The ratio of the time constants of the 80% and 100% modulation depth runs, $1.9 \text{ ms}/2.8 \text{ ms} \approx 0.68$, is within 7% of the predicted scaling $0.8^2 = 0.64$. This scaling does not hold between 40% and 80%, which have very similar growth times. A qualitative change is observed in the shape of the mode when the modulation depth is increased from 40% to 80% as shown in figure 6. At 80% modulation depth, the polar, equatorial, and mid-latitude plumes are all clearly visible. But at 40% modulation depth, only the polar plume is distinct. Figure 5c shows that although there is some outward motion at the equator, the extent of the motion is greatly reduced compared to that shown in figure 5b for 80% modulation depth.

This evidence suggests that we are observing a crossover in convection regimes where different forces are dominant. At 80% and 100% modulation depth, acoustic gravity overwhelms rotational forces and the shape of the mode is mainly determined by the spherical force field.

At 40% modulation depth, the acoustic gravity is weak enough where centripetal forces at the equator surpass acoustic ones and suppress the equatorial plume.

CONCLUSION

The relevance of our experiment to planetary or stellar convection is determined by the dimensionless fluid parameters of our system. Equation 1 may be non-dimensionalized according to $\mathbf{r} = R\mathbf{r}^*$, $\mathbf{v} = \frac{\chi}{R}\mathbf{v}^*$, $\bar{\rho} = \rho_w\bar{\rho}^*$, $\tau = \frac{R^2}{\chi}\tau^*$, and $\langle v_1^2 \rangle = v_{rms}^2 v_1^{2*}(r^*)$ where R is the bulb radius, χ is the thermal diffusivity, ρ_w is the density at the glass, v_{rms} is the root-mean-squared acoustic velocity, and the starred parameters are dimensionless. We have replaced the thermal scale here with a density scale which is more natural for our system. The resulting non-dimensional parameters are the Prandtl number $Pr = \eta/(\rho_w\chi) \simeq 0.15$, gravitational Rayleigh number $Ra_g = gR^3\rho_w/(\eta\chi) \simeq 5600$, and acoustic Rayleigh number $Ra_{ac} = v_{rms}^2 R^2\rho_w/(2\eta\chi) \simeq 3 \times 10^6$. Centripetal forces compared to Earth's gravity are parametrized by the Froude number $Fr = \Omega^2 R/g \simeq 17$ or the acoustic Froude number $Fr_{ac} = 2\Omega^2 R^2/v_{rms}^2 \simeq 0.026$, where Ω is the rotation rate. The strength of the Coriolis force is parametrized by the Ekman number $Ek = \eta/(2\rho_w\Omega R^2) \simeq 6 \times 10^{-4}$. These were evaluated with $R = 15$ mm, $\Omega = 2\pi \times 17$ Hz, $v_{rms}^2 \simeq (20 \text{ m s}^{-1})^2/2$, $\eta/\rho_w \simeq 3 \times 10^{-5} \text{ m}^2 \text{ s}^{-1}$, $\chi \simeq 2 \times 10^{-4} \text{ m}^2 \text{ s}^{-1}$ estimated from data in [18, 19]. Our peak acoustic Rayleigh number is greater than what is reported for GeoFlow [9, 30]. Although these values can be simulated [31], there is a route to upscaling this phenomenon. The plasma is excited via its absorption of the externally applied microwave field. Under the right conditions, the phase of the oscillating absorption coefficient provides a source of gain which will spontaneously amplify and sustain the sound field in the presence of convection [32].

This experiment captures some notoriously difficult aspects of convection. Namely, it is a bench-top system capable of driving thermal convection in a spherical force that overpowers Earth's gravity. The system rotates and is internally heated. It has a factor ~ 2 change in density between the inner and outer limits of the unstable region, going far beyond the Boussinesq approximation into the compressible regime [33]. The effective gravity of the acoustic mode changes sign at about half of the bulb radius, and divides the bulb into stable and unstable regions. Further, the plumes in the outer zone transport angular momentum and likely result in some amount of differential rotation. Although this experiment does not exhibit relevant magnetic fields, these features are thought to play a key role in the solar tachocline and the sun's magnetic cycle. Finally we note that on the long time scale, the processes discussed here lead to a noisy 'steady state' which is representative of conditions that

accompany blackout in communication with re-entry and hypersonic vehicles [23].

ACKNOWLEDGMENT

We acknowledge valuable discussions with Nicholas Featherstone and Jonathan Aurnou. This research was initiated with funding from the Defense Advanced Research Projects Agency (DARPA D19AP00015). S. Putterman, J. Koulakis and Y. Ofek are supported in part by the AFOSR (FA9550-21-1-0295).

The views, opinions and/or findings expressed are those of the authors and should not be interpreted as representing the official views or policies of the Department of Defense or the U.S. Government.

REFERENCES

-
- * koulakis@physics.ucla.edu
- [1] D. J. Galloway, Y. Uchida, and N. O. Weiss, Generation of coronal currents by the solar convection zone, *Publications of the Astronomical Society of Australia* **18**, 329 (2001).
 - [2] N. A. Featherstone and B. W. Hindman, The emergence of solar supergranulation as a natural consequence of rotationally constrained interior convection, *The Astrophysical Journal Letters* **830**, L15 (2016).
 - [3] P. Olson, Experimental dynamos and the dynamics of planetary cores, *Annual Review of Earth and Planetary Sciences* **41**, 153 (2013).
 - [4] S. M. Tobias, The solar dynamo, *Philosophical Transactions of the Royal Society A* **360**, 2741 (2002).
 - [5] L. D. Landau and E. M. Lifshitz, *Electrodynamics of continuous media* 2nd edition (Butterworth-Heinemann, Burlington, MA, USA, 1984) pp. 59–64.
 - [6] B. Chandra and D. E. Smylie, A laboratory model of thermal convection under a central force field, *Geophysical Fluid Dynamics* **3**, 211 (1972).
 - [7] K. Amara and J. Hegseth, Convection in a spherical capacitor, *Journal of Fluid Mechanics* **450**, 297 (2002).
 - [8] P. H. Roberts, Electrohydrodynamic convection, *Quarterly Journal of Mechanics & Applied Mathematics* **22**, 211 (1969).
 - [9] F. Zaussinger, P. Haun, P. S. Szabo, V. Travnikov, M. A. Kawwas, and C. Egbers, Rotating spherical gap convection in the GeoFlow International Space Station (ISS) experiment, *Physical Review Fluids* **5**, 063502 (2020).
 - [10] J. E. Hart, G. A. Glatzmaier, and J. Toomre, Space-laboratory and numerical simulations of thermal convection in a rotating hemispherical shell with radial gravity, *J. Fluid Mech.* **173**, 519 (1986).
 - [11] J. E. Hart, J. Toomre, A. E. Deane, N. E. Hurlburt, G. A. Glatzmaier, G. H. Fichtl, F. Leslie, W. W. Fowles, and P. A. Gilman, Laboratory experiments on planetary and

- stellar convection performed on Spacelab 3, *Science* **234**, 61 (1986).
- [12] P. Beltrame, V. Travnikov, M. Gellert, and C. Egbers, GEOFLOW: simulation of convection in a spherical shell under central force field, *Nonlinear Processes in Geophysics* **13**, 413 (2006).
- [13] M. Gellert, P. Beltrame, and C. Egbers, The GeoFlow experiment: spherical Rayleigh-Bénard convection under the influence of an artificial central force field, *J. Phys.: Conf. Ser.* **14**, 157 (2005).
- [14] J. T. Karlsen, P. Augustsson, and H. Bruus, Acoustic force density acting on inhomogeneous fluids in acoustic fields, *Physical Review Letters* **117**, 114504 (2016).
- [15] J. P. Koulakis, S. Pree, A. Thornton, A. S. Nguyen, and S. Putterman, Pycnoclinic acoustic force, *Proceedings of Meetings on Acoustics* **34**, 045005 (2018).
- [16] J. P. Koulakis and S. Putterman, Convective instability in a stratified ideal gas containing an acoustic field, *Journal of Fluid Mechanics* **915**, A25 (2021).
- [17] G. Z. Gershuni and D. V. Lyubimov, *Thermal vibrational convection* (John Wiley & Sons Ltd., West Sussex, England, 1998) pp. 249–250.
- [18] J. P. Koulakis, S. Pree, A. L. F. Thornton, and S. Putterman, Trapping of plasma enabled by pycnoclinic acoustic force, *Physical Review E* **98**, 043103 (2018).
- [19] J. P. Koulakis, S. Pree, and S. Putterman, Acoustic resonances in gas-filled spherical bulb with parabolic temperature profile, *Journal of the Acoustical Society of America* **144**, 2847 (2018).
- [20] S. Lepot, S. Aumaitre, and B. Gallet, Radiative heating achieves the ultimate regime of thermal convection, *PNAS* **115**, 8937 (2018).
- [21] D. Goluskin, *Internally Heated Convection and Rayleigh-Bénard Convection* (Springer International Publishing, Switzerland, 2016).
- [22] S. Pree, J. Koulakis, A. Thornton, and S. Putterman, Acousto-convective relaxation oscillation in plasma lamp, *Proceedings of Meetings on Acoustics* **34**, 045015 (2018).
- [23] J. P. Koulakis, S. Pree, and S. Putterman, Generation and characterization of chaotic convection in collisional plasma, *IEEE Transactions on Plasma Science* **48**, 3840 (2020).
- [24] J. P. Koulakis, A. L. F. Thornton, and S. Putterman, Magnetron coupling to sulfur plasma bulb, *IEEE Transactions on Plasma Science* **45** (2017).
- [25] G. Courret, P. Nikkola, S. Wasterlain, O. Gudozhnik, M. Girardin, J. Braun, S. Gavin, M. Croci, and P. W. Egolf, On the plasma confinement by acoustic resonance - an innovation for electrodeless high-pressure discharge lamps, *Eur. Phys. J. D* **71**, 214 (2017).
- [26] C. W. Johnston, H. W. P. van der Heijden, G. M. Janssen, J. van Dijk, and J. J. A. M. van der Mullen, A self-consistent LTE model of a microwave-driven, high pressure sulfur lamp, *J Phys. D: Appl. Phys* **35**, 342 (2002).
- [27] C. W. Johnston, H. W. P. van der Heijden, A. Hartgers, K. Garloff, J. van Dijk, and J. J. A. M. van der Mullen, An improved LTE model of a high pressure sulfur lamp, *J Phys. D: Appl. Phys* **37**, 211 (2004).
- [28] B. P. Turner, M. G. Ury, Y. Leng, and W. G. Love, Sulfur lamps - progress in their development, *Journal of the Illuminating Engineering Society* **26**, 10 (1997).
- [29] A. Zebib, G. Schubert, J. L. Dein, and R. C. Paliwal, Character and stability of axisymmetric thermal convection in spheres and spherical shells, *Geophys. Astrophys. Fluid Dynamics* **23**, 1 (1983).
- [30] B. Futterer, C. Egbers, N. Dahley, S. Koch, and L. Jehring, First identification of sub- and supercritical convection patterns from ‘GeoFlow’, the geophysical flow simulation experiment integrated in Fluid Science Laboratory, *Acta Astronautica* **66**, 193 (2010).
- [31] T. Gastine, J. Wicht, and J. M. Aurnou, Turbulent Rayleigh-Bénard convection in spherical shells, *J. Fluid Mech* **778**, 721 (2015).
- [32] S. Pree, S. Putterman, and J. P. Koulakis, Acoustic self-oscillation in a spherical microwave plasma, *Physical Review E* **100**, 033204 (2019).
- [33] R. Menaut, Y. Corre, L. Huguet, T. L. Reun, T. Alboussière, M. Bergman, R. Deguen, S. Labrosse, and M. Moulin, Experimental study of convection in the compressible regime, *Physical Review Fluids* **4**, 033502 (2019).